

ULRR

Influence of quenching and aging on residual stress in Al-Zn-Mg-Cu alloy 7449

| | |
|---------------|---|
| Item Type | Article |
| Authors | Robinson, Jeremy;Tanner, David;Van Petegem, S.;Evans, A. |
| Citation | Maney Publishing;28 (4), pp. 420-430 |
| Publisher | Maney Publishing |
| Download date | 2026-04-16 07:51:00 |
| Item License | https://creativecommons.org/licenses/by-nc-sa/1.0/ |
| Link to Item | https://hdl.handle.net/10344/3778 |

The influence of quenching and aging on residual stress in the Al-Zn-Mg-Cu alloy 7449.

J.S.Robinson¹, D.A.Tanner¹, S. Van Petegem², A. Evans³

¹ Materials Surface Science Institute, University of Limerick, Limerick, Ireland

² Materials Science and Simulations, Paul Scherrer Institut, CH-5232 Villigen, Switzerland

³ Institut Laue Langevin, 6 rue Jules Horowitz, Grenoble, France

Corresponding author

J.S. Robinson

Materials Surface Science Institute, University of Limerick, Ireland.

Email; jeremy.robinson@ul.ie

Telephone; +353 61 202240

Fax; +353 61 338172

Abstract

This investigation aimed to quantify the size and distribution of residual stresses remaining in rectilinear aluminium forged alloy blocks after they had been partially and fully heat treated. Various quench conditions were used including water at different temperatures and poly oxyethylene glycol (PAG) in two concentrations. The influence of standard and novel aging procedures including retrogression and reaging has been determined. Residual stresses were characterised using x-ray and neutron diffraction. Residual stress magnitudes were found to vary significantly with rapidity of cooling from the solution treatment temperature with the subsequent aging treatments having a much smaller effect. The influence of the heat treatments on mechanical properties of the alloy was predicted by means of quench factor analysis and measured using indentation hardness and tensile testing. Quench factor analysis is also used to predict the change in lattice parameter arising from different quench paths in the strain free reference samples (d^0).

Keywords

Residual stresses; neutron diffraction; heat treated aluminium alloy; synthetic quenchant; quench factor analysis.

Introduction

An unfortunate consequence of the heat treatment of precipitation hardened aluminium alloys is the introduction of high magnitude residual stresses. Severe thermal gradients arise when quenching rapidly from the solution heat treatment temperature. These gradients cause inhomogeneous plastic flow to occur which in turn produces distortion and residual stresses. One of the first descriptions of the magnitude of the residual stresses in heat treatable aluminium alloys was provided by Kleint and Janney¹. More recently Becker, Karabin et al.² quantified both the residual stresses and subsequent distortion for aluminium alloy bars when water quenching. For a rectilinear block like those investigated here, immediately after quenching tensile plastic strains occur initially at the rapidly cooling edges of the material. The plastic zone then expands to cover all the rapidly cooling surfaces. The block at this point consists of a soft hot interior surrounded by a harder and cooler exterior stretched shell. As the central region starts to cool, it tries to contract but is constrained by the hard outer shell and undergoes tensile plastic deformation. As the block cools further, the magnitude of surface plastic strains diminish as a compressive stress is developed, finally resulting in a surface stressed into compression and a centre into tension as demonstrated by the early finite element modelling of Jeanmart and Bouvaist³ and the neutron diffraction measurements made by Yazdi, Reira et al.⁴ and Walker and Hom⁵. The final stress pattern is a reflection of the geometry of the component and of the temperature gradients generated throughout in the quench.

After rapid quenching, the residual stresses are so large that most commercial products must be stress relieved. Annealing type methods of relieving stress are not usually appropriate for precipitation hardened alloys as the temperature to effect major stress relief will be well above the aging temperature. This was illustrated by Orner and Kulin⁶ who demonstrated concomitant softening associated with stress relieving thermal treatments in precipitation hardened aluminium alloys. For simple configurations, significant stress relief can be induced by applying plastic deformation using stretching or cold compression immediately *after* quenching while the material is in a soft condition. One of the few quantitative investigations of the application of cold work to solution treated aluminium alloys was performed by Altschuler, Kaatz et al.⁷ who demonstrated its efficacy in significantly reducing residual stress. This investigation and those of Nickola⁸ and Koc, Culp et al.⁹ highlighted the geometrical limitations of applying cold work, and for complex shapes this approach is often not possible. The alternative is to reduce the residual stresses arising from heat treatment by slowing down the rate of cooling during quenching. This can be achieved by increasing the water temperature (up to boiling water), changing the quench media or changing the surface finish. The disadvantage of this approach is the increased level of precipitation that can occur during quenching which in turn reduces the subsequent aging response, the degree being dependent on the quench sensitivity of the alloy in question.

After quenching, precipitation results in a large increase in strength. This aging can be at room temperature where it is known as natural aging, or artificial aging when performed at elevated temperatures. Precipitation of coherent

and semi-coherent second phases can itself cause micro strains around and within the precipitates but the resulting stresses affect a volume too small to alleviate macro stresses or cause additional issues with the bulk material.

No residual stress relaxation is observed during natural aging as shown by the long term residual stress measurements made by Tanner, Robinson et al. ¹⁰ as shown in Figure 1. They followed the long term natural aging of a cold water quenched specimen of 7010. The sample size was 60 x 60 x 15 mm and was quenched from a solution treatment temperature of 470±5 °C. The surface residual stresses were determined using the standard $\text{Sin}^2\psi$ technique on a laboratory x-ray diffractometer. The plotted error bars are ±3 standard deviations, calculated from the straight line fit of the d ($\{422\}$ interplanar spacing) versus $\text{Sin}^2\psi$ plots. The time plotted is calculated as the time from quenching to the mid-point of time during the residual stress measurement.

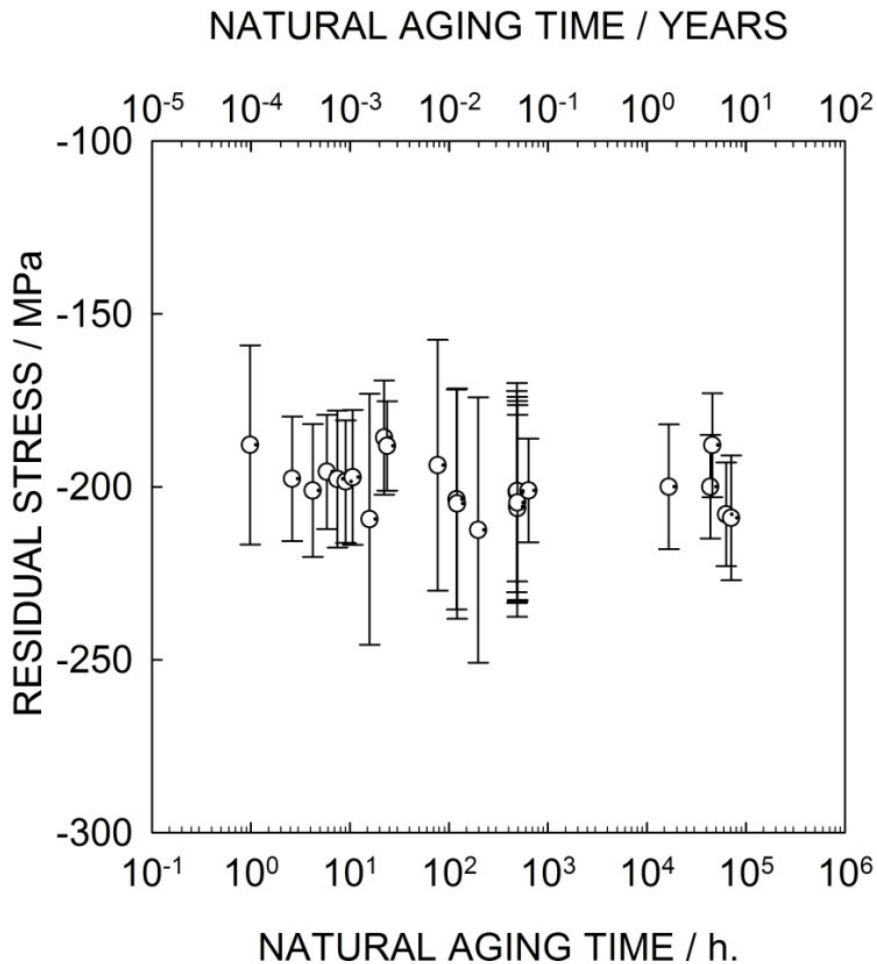


Figure 1. Stability of surface residual stresses at room temperature for cold water quenched 7010 characterised by x-ray diffraction. Error bars correspond to ±3 standard deviations, calculated from the straight line fit of the $d_{\{422\}}$ versus $\text{Sin}^2\psi$ plots.

Artificial aging temperatures depend upon the alloy type and the degree of precipitation required to bring about the necessary balance of mechanical properties in a sensible period of time. The artificial aging treatments applied to alloys are usually in the range 120-190°C. These temperatures are high enough to allow some dislocation motion and macro stresses can be relieved but the amount of relaxation is small and difficult to quantify. This should not be surprising as the point of aging treatments is to make dislocation glide much more difficult. In general the precipitation treatments used to obtain the peak aged (T6) and overaged (T7) tempers provide only modest reduction in stresses, at best ranging from about 10 to 35% as suggested by Davis, Davidson et al. ¹¹. Retrogression and reaging type thermal treatments are applied to certain thin section 7000 series alloys to improve the balance of strength and stress corrosion/exfoliation corrosion resistance. They incorporate an additional short duration (normally less than one hour) aging step at a temperature between 180 and 220°C. As such the cumulative effect of time at temperature may result in a small additional amount of stress relaxation. Evidence for residual stress relaxation in aged material is very limited. However, Cina, Kaatz et al. ¹² did quantify the change in residual stresses for aluminium alloys by monitoring the variation in the radius of shot peened plates during aging treatments.

This investigation aimed to quantify the magnitude and distribution of residual stresses remaining in rectilinear aluminium alloy blocks after they had been quenched and aged. Various quench conditions were used including water at three different temperatures and poly oxyethylene glycol (PAG) in two concentrations, the objective being to significantly vary the heat transfer coefficient during quenching. The influence of standard and novel aging procedures (retrogression and reaging) has also been determined. Residual stresses were characterised using both x-ray and neutron diffraction and were linked to the resulting mechanical properties when assessed using indentation hardness and tensile testing. The quench sensitivity of the 7449 alloy for an overaged condition has been characterised. The term quench sensitivity is a relative measure of the degree of precipitation occurring during quenching from the solution heat treatment temperature as described by Staley¹³. Quench factor analysis (QFA) has also permitted the prediction of the variation in indentation hardness arising from the different quench paths. It has been demonstrated that quench factor analysis is capable of predicting the change in lattice parameter arising from different quench paths in the strain free reference samples (d^0) used for the neutron diffraction measurements.

Experimental procedures

Material details

This experiment used consistent sized rectilinear blocks of the very high strength Al-Zn-Mg-Cu aerospace alloy 7449. The blocks were cut from a section of a large triaxially open die forged aircraft spar type forging. The forging was manufactured from a solid cylindrical cast ingot of 7449 alloy. The blocks were chemically and mechanically homogeneous. The composition of the 7449 alloy is given in Table 1.

Table 1. Specification alloy chemistry and chemical analysis (ca) results, wt%

| Alloy | Si | Fe | Cu | Mn | Mg | Zn | Ti+Zr | Al |
|-----------|-------------|-------------|-------------|-------------|---------|-------------|-------------|------|
| 7449 | 0.12 max | 0.15 max | 1.4- 2.1 | 0.20 max | 1.8-2.7 | 7.5- 8.7 | 0.25 max | Bal. |
| 7449 (ca) | 0.06 | 0.08 | 2.02 | 0.01 | 1.92 | 8.39 | 0.138 | Bal. |

The block dimensions prior to heat treatment were 50 mm (L-longitudinal) × 80 mm (LT-long transverse) × 127 mm (ST-short transverse) where the orientations refer to those of the original primary working directions as illustrated in Figure 2. The longitudinal direction has been arbitrarily designated x, the long transverse y and the short transverse z. Blocks were heat treated as pairs, with one of the pairs used to provide strain free (d^0) samples. These sacrificial blocks were also used to fabricate tensile tests to determine the influence of the heat treatment on the tensile mechanical properties. The microstructure of the blocks, determined using optical metallography consisted of approximately rod shaped grains elongated into the longitudinal direction with a typical grain length being <1000 μm . In the transverse directions, the grain characteristic dimension was <200 μm . Within these grains a substructure was observed consisting of well defined polygonised equiaxed subgrains. The diameter of the subgrains was <20 μm . Other coarse phases noted were fragmented Al-Cu-Fe constituent particles and a very small volume fraction of undissolved MgZn_2 .

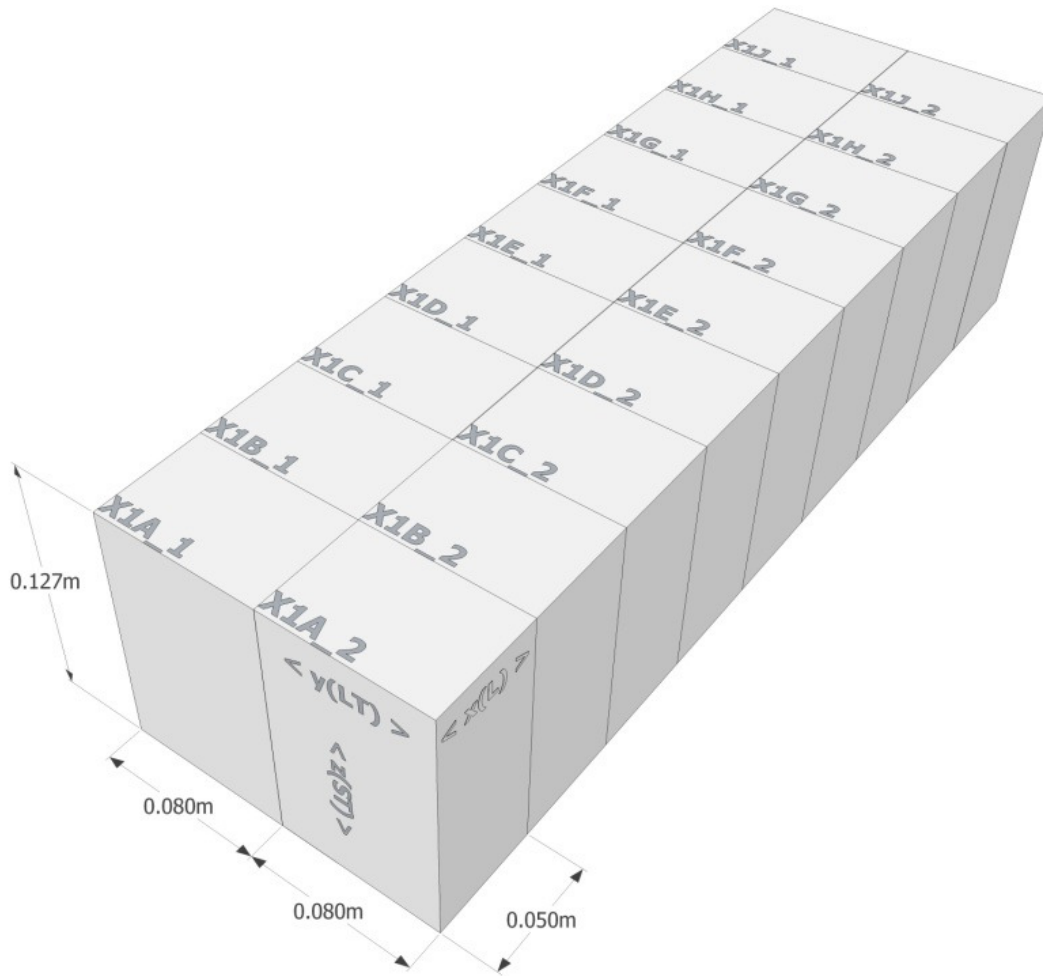


Figure 2. Forging prior to sectioning into 18 rectilinear blocks. The *L*, *LT* and *ST* directions correspond to the principal working directions arising from triaxial forging.

The blocks were solution heat treated at $470 \pm 5^\circ\text{C}$ and then rapidly quenched by immersing into the quench media with accompanied vigorous agitation where possible (block moved through the liquid at $\sim 1 \text{ m s}^{-1}$). Each block had a mass of approximately 1.35kg with a surface area of 0.04 m^2 . The Biot number for the cold water quench was approximately 0.8. The Biot number is a dimensionless number that gives an index of the ratio of the heat transfer resistances inside and at the surface of a body. If the Biot number is > 0.1 then the thermal gradients are significant within the body and will give rise to inhomogeneous thermal contraction. The Biot number was calculated using a characteristic linear dimension for the block of 12 mm (ratio of block volume to surface area), an average thermal conductivity of $180 \text{ W m}^{-1}\text{K}^{-1}$ and an average heat transfer coefficient of $12,000 \text{ W m}^{-2}\text{K}^{-1}$ calculated from quenching experiments. The surface condition of the blocks was a uniform smooth milled surface. Representative cooling curves were recorded using an additional block containing two 1.5 mm diameter shrouded type K thermocouples. Thermocouples were located at position A, as shown in Figure 3, and within 1 mm of the centre of the surface defined by the *x* and *y* directions; close to position D. Temperatures were recorded at 10 Hz during quenching.

After completion of quenching, precipitation heat treatments were carried out as detailed in Table 2.

Table 2. Heat treatment codes, details of the type of quench media and temperature, and the subsequent aging conditions used prior to neutron diffraction (nd) and tensile testing (tt). W = unstable aging at room temperature, UA = under aging (48h at 120°C), OA = over aging (6 h at 120°C +10h at 160°C).

| Block code | Heat treatment code | Quench details | Aging details |
|------------|---------------------|---|--------------------|
| X1A_1 | CWQ | Cold water immersion ($< 20^\circ\text{C}$) | W (nd) and OA (tt) |
| X1A_2 | | | |
| X1B_1 | Q60 | Warm water immersion (60°C) | W (nd) and OA (tt) |
| X1B_2 | | | |

| | | | |
|-------|--------|---|--|
| X1C_1 | BWQ | Boiling water immersion (100°C) | W (nd) and OA (tt) |
| X1C_2 | | | |
| X1D_1 | RRA200 | Cold water immersion (<20°C) | 48h at 120°C + 500s at 200°C + 48h at 120°C (nd and tt) |
| X1D_2 | | | |
| X1E_1 | PAG16 | Poly oxyethylene glycol 16% immersion(<20°C) | W (nd) and OA (tt) |
| X1E_2 | | | |
| X1F_1 | PAG30 | Poly oxyethylene glycol 30% immersion (<20°C) | W (nd) and OA (tt) |
| X1F_2 | | | |
| X1G_1 | UA | Cold water immersion (<20°C) | 48h at 120°C (nd and tt) |
| X1G_2 | | | |
| X1H_1 | OA | Cold water immersion (<20°C) | 6 h at 120°C +10h at 160°C (nd and tt) |
| X1H_2 | | | |
| X1J_1 | RRA240 | Cold water immersion (<20°C) | 48h at 120°C + 100s at 240°C + 48h at 120°C (nd and tt) |
| X1J_2 | | | |

The experimental variables investigated were the quench media and temperature, and the subsequent aging procedure. Water at room temperature and 60°C, boiling water and a commercial grade poly oxyethylene glycol (PAG) in two concentrations were investigated (Houghton Products Aqua-Quench 251). Natural aging at room temperature (referred to as unstable aging or the W temper), under-aging (UA, 48 hours at 120°C), over-aging (OA, 6 hours at 120°C +10 hours at 160°C) and retrogression and reaging (RRA) treatments at 200 and 240°C formed the aging investigation.

X-ray diffraction

Residual stress measurements using a $\text{Sin}^2\psi$ technique were performed on a Philips X'Pert x-ray diffractometer using Cu K α radiation operating in the ω configuration. The measurement procedures followed were those documented in the best practice guide published by Fitzpatrick, Fry et al.¹⁴. The position of the peak arising from diffraction from the Al {422} planes was measured ($136^\circ < 2\theta < 139^\circ$). Sixteen scans were performed for each stress measurement using different ψ values within the range $0 \leq \psi \leq 60^\circ$ (positive tilting only, ψ - angle between the surface normal and the bisector of source and diffracted x-ray beam). Certain scans were repeated using positive and negative tilting ($-60 \leq \psi \leq 60^\circ$). The resulting spectra were analysed using Philips PC-Stress Software (version 2.61) with peak locations determined using a Pearson VII fitting technique. In all cases these sixteen peak positions were used to calculate the straight line d (lattice spacing) versus $\text{Sin}^2\psi$ plots. The calculation of residual stress from the measured peak position was made using the theory supplied by Noyan and Cohen¹⁵. The elastic constants were taken from literature for the {422} planes as provided by Hauk and Macherauch¹⁶. A total of seven measurements were made on each block, each measurement being made in a different location but close to either position B or C as shown in Figure 3. The average of these seven measurements is reported. The component of surface residual stress sampled was the σ_{zz} in all cases (residual stress in the ST direction). The irradiated area was in the form of a line approximately 2mm thick (in the z direction) and 12 mm long (in the y direction). The penetration depth of the x-rays was assumed to be of the order of 100 μm calculated using reference data contained in Cullity and Stock¹⁷

Neutron diffraction

Residual strains were measured using the time-of-flight neutron diffractometer POLDI (Pulse-OverLap Diffractometer) located at SINQ at the Paul Scherrer Institut in Villigen, Switzerland. The method of operation of this

instrument is described by Stuhr, Grosse et al.¹⁸. Recent measurements made by Drezet and Phillion¹⁹ on large direct chill cast aluminium ingots has confirmed this instrument's suitability for measuring residual stresses in thick aluminium alloy products. Measurements were made following the guidelines present in^{20, 21, 22}. The sampling gauge volume was set at $3.8 \times 3.8 \times 3.8 \text{ mm}^3$ as defined by the incident slit widths and the diffracted beam radial collimator. The incident slits were advanced as far as possible to minimise vertical divergence and this was estimated to result in an increase of the vertical dimension of the gauge volume to 4.5 mm. In the horizontal plane there was negligible divergence due to focussing of the beam. As POLDI is a time-of-flight instrument the position of multiple diffraction peaks with coincidental scattering vectors are measured. This permitted the use of a full diffraction pattern type analysis as first described by Pawley²³. The full pattern refinement leads to the determination of an average lattice parameter, a_i based upon the position of all available peaks, where i is the sampled direction relative to the specimen; $i=x,y,z$. The refinement enabled the calculation of the lattice parameter using reflections from up to five sets of interplanar spacings (mainly the {111}, {200}, {400}, {311}, and {422} although this was sample and orientation dependent). This has the potential to reduce the effects of elastic anisotropy (small for aluminium) and the influence of plastic anisotropy due to intergranular strains. Conducting a {311} single peak analysis indicated that the difference in residual stress between this analysis and the full pattern refinement was small. This is consistent with other studies since the {311} reflection tends to exhibit low intergranular strains.

Three positions within each block were sampled as shown in Figure 3, and the same measurement locations were used for each block so that the measurements could be directly compared. In addition, three orthogonal line scans were made on the cold water quenched block (X1A1) only. The measurements originated from the vertex at the centre of the block, moving out to the faces with the directions following the primary mechanical working directions $x(L)$, $y(LT)$ and $z(ST)$ as shown in Figure 3.

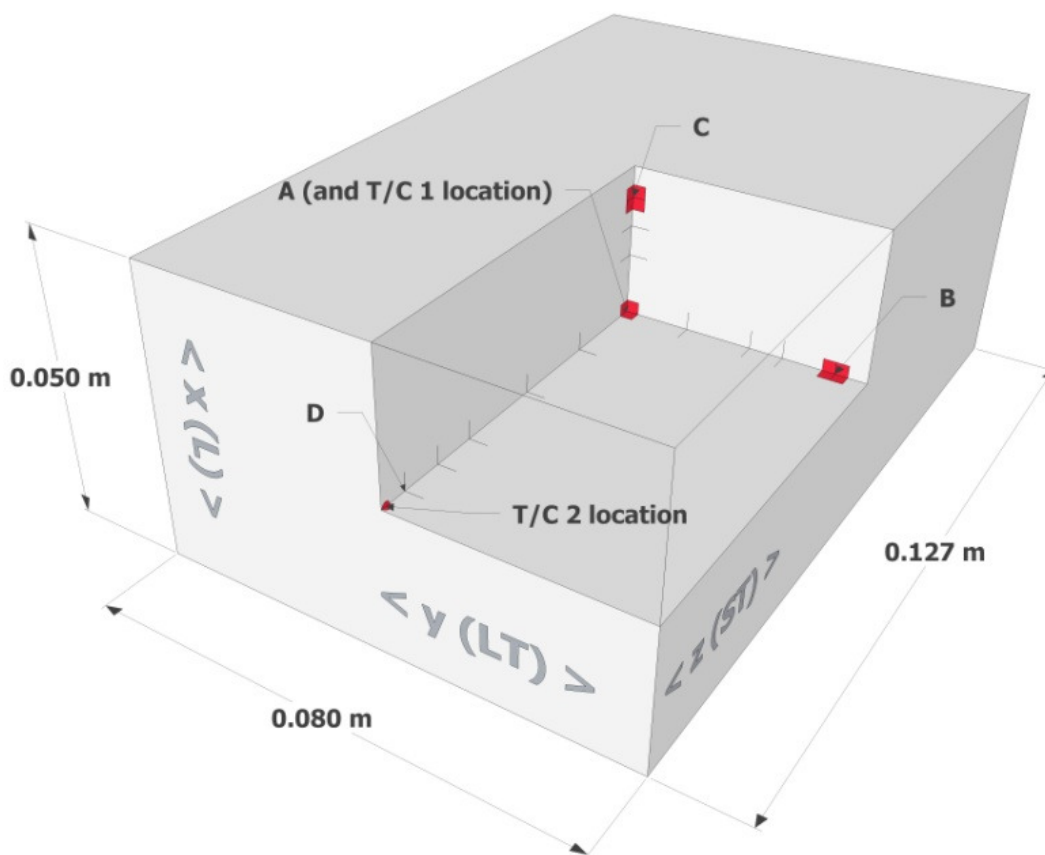


Figure 3. Neutron diffraction measurement locations, A, B C and D (d^0 only), and thermocouple locations for measurement of cooling curves during quenching. Additional line scan measurement locations originating at the central vertex are for the cold water quenched block (X1A1) only.

The residual strains were measured at the geometrical centre of the blocks (position A) and then 2 further measurement with the centre of the gauge volume located 7 mm below the surface defined by the $x(L)$ and $z(ST)$ directions (position B), and 7 mm below the surface defined by the $y(LT)$ and $z(ST)$ directions (position C). The strain at each location was measured in three orthogonal directions corresponding to the primary working directions of the forging. These directions were assumed to be the principal stress directions. Lattice spacings were converted to residual strains and stresses using the standard three dimensional Hooke's law as shown in the equations below. and

given in Hutchings, Withers et al. ²⁴. A Young's modulus of 70 GPa and a Poisson's ratio of 0.3 was used in all the calculations.

$$\sigma_{xx} = \frac{E}{1+\nu} \epsilon_{xx} + \frac{E\nu}{(1+\nu)(1-2\nu)} (\epsilon_{xx} + \epsilon_{yy} + \epsilon_{zz}) \quad (1)$$

$$\sigma_{yy} = \frac{E}{1+\nu} \epsilon_{yy} + \frac{E\nu}{(1+\nu)(1-2\nu)} (\epsilon_{xx} + \epsilon_{yy} + \epsilon_{zz}) \quad (2)$$

$$\sigma_{zz} = \frac{E}{1+\nu} \epsilon_{zz} + \frac{E\nu}{(1+\nu)(1-2\nu)} (\epsilon_{xx} + \epsilon_{yy} + \epsilon_{zz}) \quad (3)$$

The strain free reference samples (for measuring d^0) consisted of the square section post extracted from the centre of the sacrificial blocks. The post was separated from the blocks after heat treatment to form a right square prism of material of dimensions 10 mm (x,L) x 10 mm (y, LT) x 100 mm (z, ST). One end of the post corresponded to an external surface while the other was from deep within the block. The location of the strain free prism and the tensile test samples is shown in Figure 4.

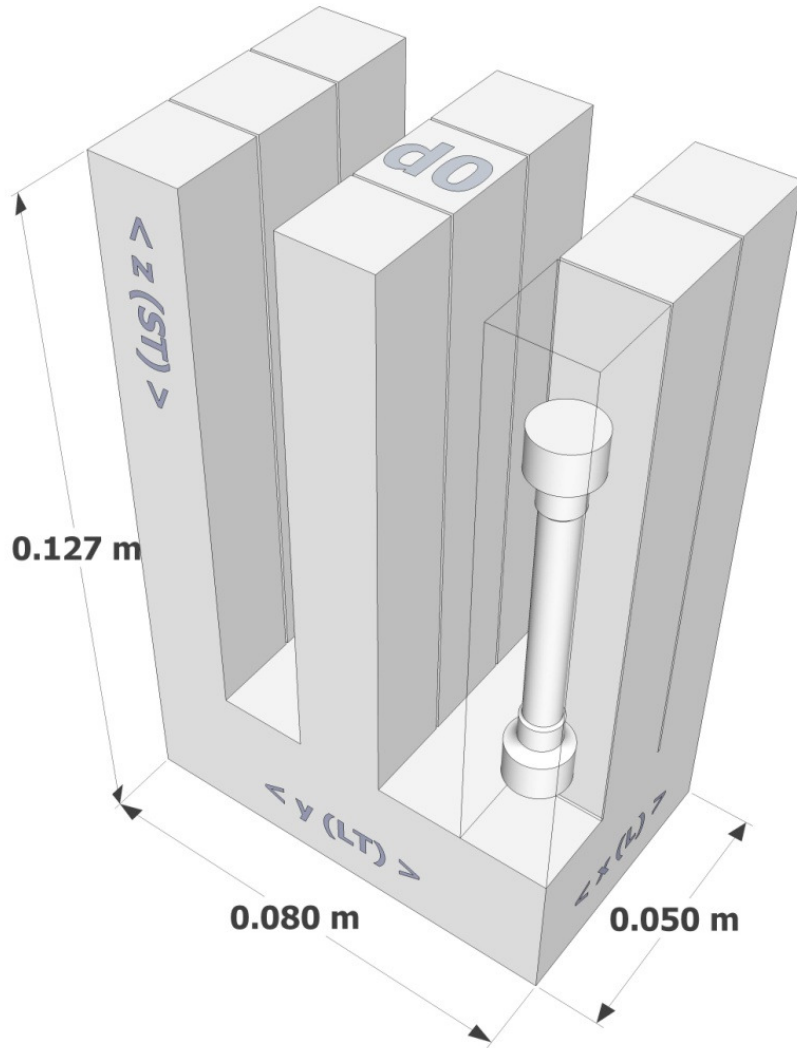


Figure 4. Cut up description of the sacrificial duplicate blocks. The location of the strain free right square prism is indicated. The remaining pieces were used for tensile test samples as illustrated.

The lattice parameter of the d^0 samples was measured at locations corresponding to A and D in Figure 3. Multiple measurements were made at each location in all three orthogonal directions to assess repeatability. Measurements were made at both A and D as a microstructural change was expected to occur in the strain free sample as the cooling rate during quenching varied from one end of the post to the other. This effect can be significant as illustrated by Steuwer, Dumont et al. ²⁵ for friction stir welds in the alloy 7010.

Tensile testing and indentation hardness testing

Tensile testing was performed in accordance with ASTM B557–84, using round specimens of gauge length 30 mm and diameter 6 mm, on a 500 kN servo hydraulic load frame utilising a 25 mm gauge length extensometer. Specimens were tested at a strain rate of $3 \times 10^{-3} \text{ s}^{-1}$ and were loaded in the z (ST) direction as shown in Figure 4. Samples from blocks that did not receive an artificial aging treatment as part of their heat treatment received about 100 days of natural aging at room temperature prior to testing. Tensile samples from these blocks were also overaged after sectioning from the block. Uncertainties in the 0.1% proof stress and tensile strength were ± 10 MPa. Two samples were tested at each condition and the average calculated and reported. Vickers hardness testing was conducted using standard equipment calibrated with a test block to the requirements of ASTM E92–92.

Results

Residual stress observations

The residual stresses present in the cold water quenched block X1A1 are shown in Table 3 with additional data from the line scans presented in Figure 5, Figure 6 and Figure 7. Both neutron diffraction and surface x-ray observations are included in the table. The centre of the block, position A in Figure 3, was in a state of triaxial tension while positions B and C exhibited compressive stresses in the directions corresponding to the orthogonal in plane directions of the neighbouring face of the block, and a tensile stress in the direction normal to these faces. (These tensile stresses are those that should tend to zero as the free surface is approached.) The larger magnitude surface residual stresses, as determined by x-ray diffraction, suggests the presence of steep residual stress gradients as the surface is approached. These steep residual stress gradients are typical and seen in other geometries as shown by Robinson, Hossain et al. ²⁶ who quantified residual stresses in much larger cold water quenched rectilinear forgings also made from 7449. Multiple (repeatability) neutron diffraction measurements on X1A1 and the associated stress free sample allowed an estimation of one standard deviation random uncertainties as ± 25 MPa. This error was larger than the in quadrature sample and d^0 peak fitting combined uncertainties. For the x-ray measurements, the one standard deviation random uncertainties were approximately ± 15 MPa.

Table 3. Residual stresses present in the cold water quenched block X1A1 as determined by neutron diffraction and x-ray diffraction. Neutron diffraction and x-ray diffraction random uncertainties were estimated at ± 25 MPa and ± 15 MPa respectively.

| | Neutron diffraction residual stress / MPa | | | X-ray residual stress / MPa |
|-------------------------|---|---------------|---------------|-----------------------------|
| LOCATION (see Figure 3) | σ_{xx} | σ_{yy} | σ_{zz} | σ_{zz} |
| A | 18 | 194 | 260 | |
| B | -120 | 61 | -70 | -211 |
| C | 72 | -190 | -79 | -222 |

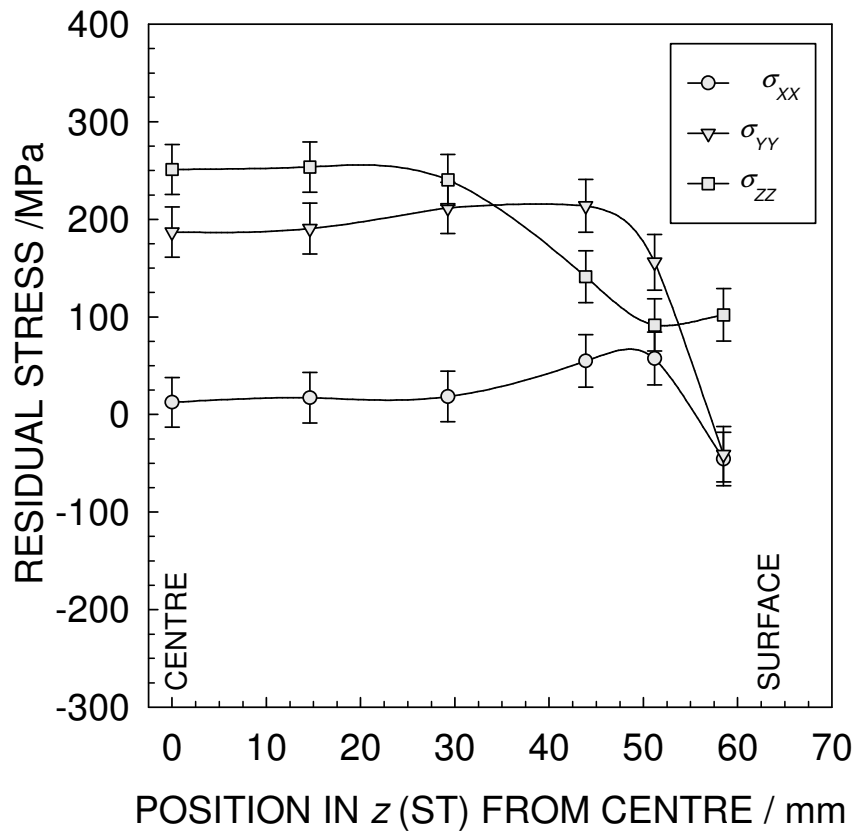


Figure 5. Residual stresses in the cold water quenched block (X1A1) measured from the central vertex out towards position D (as shown in Figure 3). The σ_{zz} component should tend to zero as the surface is approached.

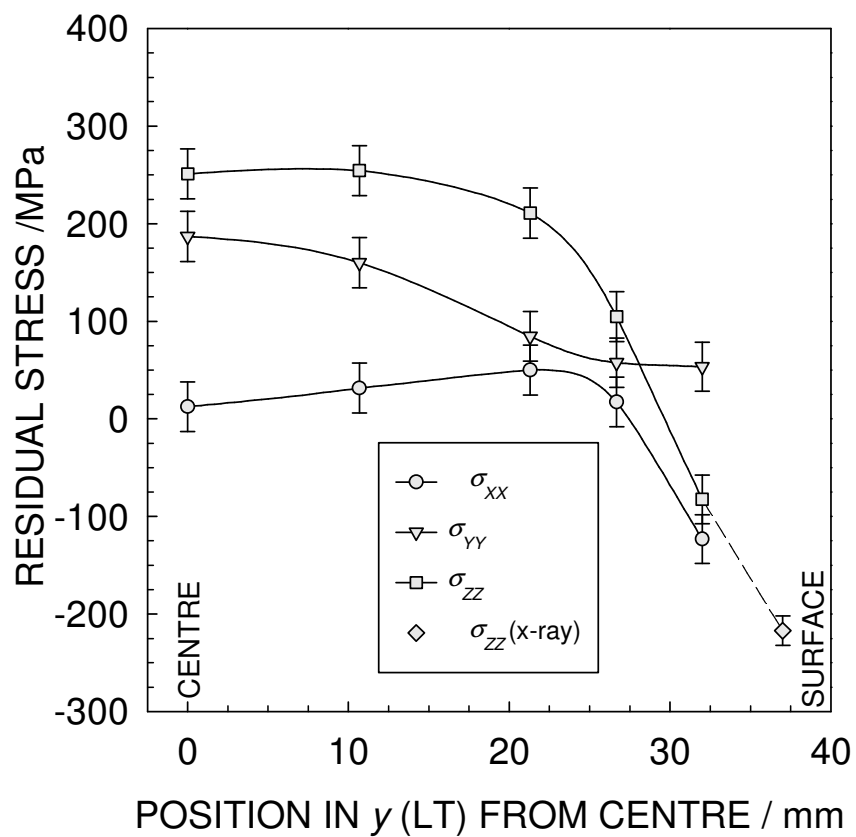


Figure 6. Residual stresses in the cold water quenched block (X1A1) measured from the central vertex out towards position B (as shown in Figure 3). The σ_{yy} component should tend to zero as the surface is approached.

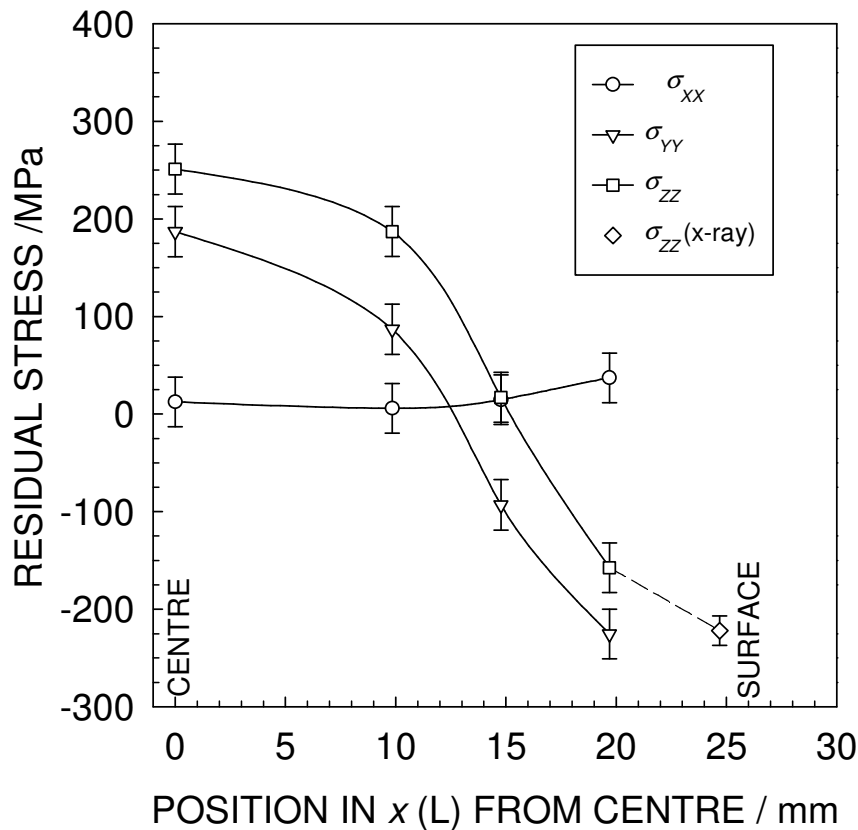


Figure 7. Residual stresses in the cold water quenched block (X1A1) measured from the central vertex out towards position C (as shown in Figure 3). The σ_{xx} component should tend to zero as the surface is approached.

Regarding the variation of the lattice parameter within the strain free reference samples, neutron diffraction measurements were made in all three orthogonal directions at the centre of the posts at a position equivalent to A in Figure 3 and similarly at position D. The differences between these measurements were insignificant and were encompassed by the (strain equivalent) random uncertainties quoted above. For this reason a single d^0 value was used in the residual stress calculations for each block. However, there was a systematic variation in the d^0 caused by the different thermal treatments. This is indicated in Figure 8 which displays the differences in the lattice parameter measured in the y (LT) direction, converted to microstrain using the cold water quenched sample as a datum. All the thermal treatments would have resulted in some loss of solute relative to the cold water quenched sample and this would be expected to be manifest as a smaller lattice parameter. In fact, the lattice parameters of the naturally aged strain free samples were all the same and encompassed by the random uncertainties except for the boiling water quenched sample which did display a significantly smaller lattice parameter. The neutron diffraction results were also in agreement with surface measurements of lattice parameter made by x-ray diffraction (labelled as X-ray NA in Figure 8). The x-ray lattice parameters were calculated from the intercept at $\text{Sin}^2\psi = 0$ in the d versus $\text{Sin}^2\psi$ plots. Artificial aging resulted in a large reduction in lattice parameter in all cases as confirmed by both neutron diffraction and x-ray measurements.

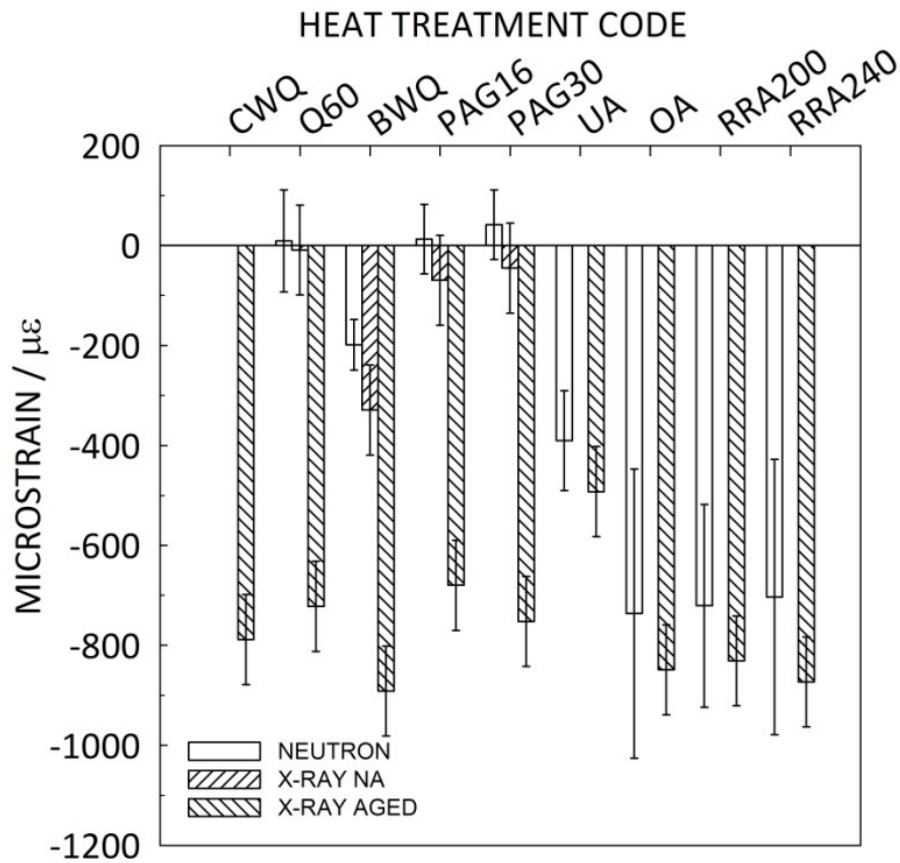


Figure 8. Differences in the lattice parameter measured in the y (LT) direction from position A of the strain free reference prisms, converted to microstrain using the cold water quenched sample as the datum. Q60 (X1B2), BWQ (X1C2), PAG16 (X1E2) and PAG30 (X1F2) were naturally aged only when assessed by neutron diffraction. X-ray measurements of the lattice parameters converted to microstrain also shown.

The pattern of residual stress distribution described in Table 3 was repeated in all of the blocks. The influence of the thermal treatments on the residual stresses present at the centre and surface locations of all the samples is shown Figure 9. The thermal treatments that significantly affect the cooling rate during quenching have the largest influence on the residual stresses. Quenching into boiling water results in a stress free block and PAG quenching also significantly reduces the residual stresses. However, warm water quenching is less effective. In contrast, the aging treatments investigated have only a minor influence on the residual stresses. The percentage reduction in residual stress relative to the cold water quenched block is presented in Figure 10. Here again the efficacy of lowering the cooling rate during quenching can be seen in contrast to the limited residual stress reduction associated with precipitation heat treatments.

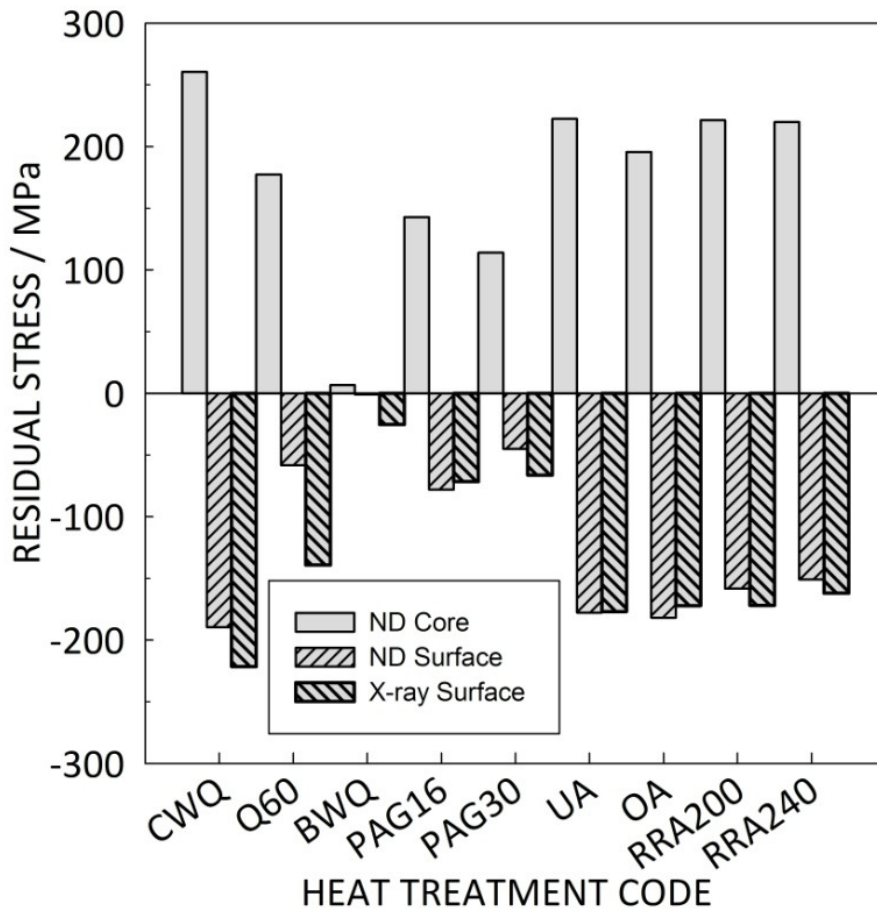


Figure 9. Residual stress magnitudes (σ_{zz} for core) present at the centre and the surface of the blocks as determined by both neutron and x-ray diffraction. (See Table 2 for HT code)

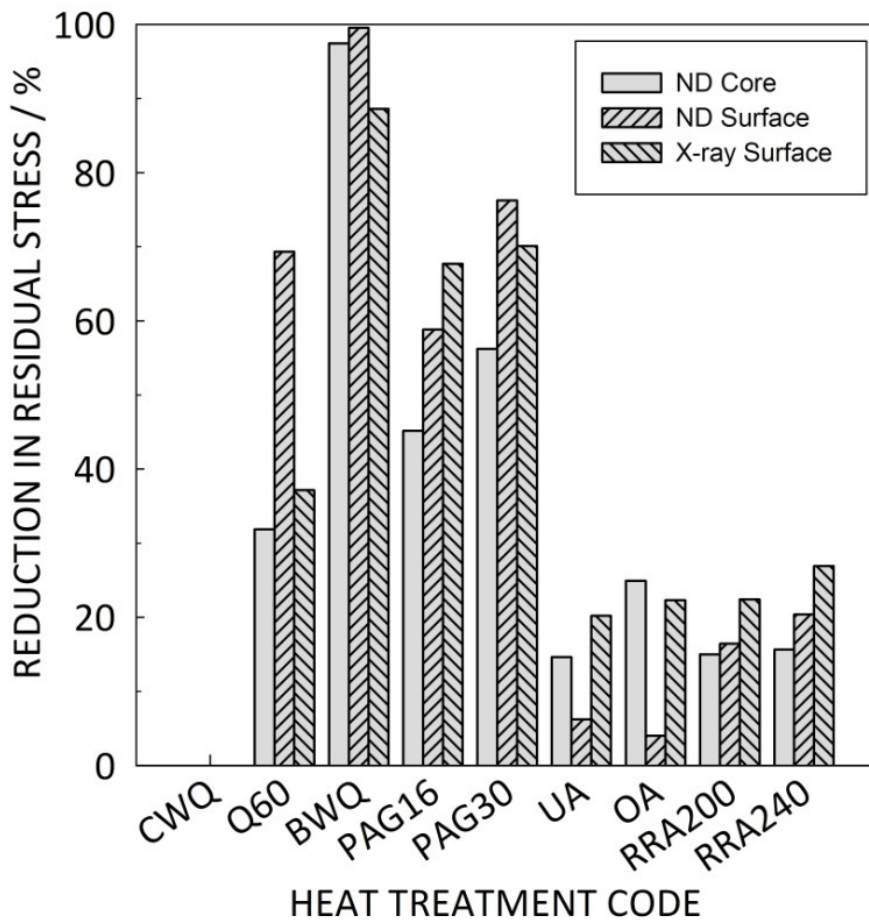


Figure 10. Relative reduction in residual stress compared to the cold water quenched sample. (See Table 2 for HT code)

Cooling during quenching and quench factor analysis

The Biot number for the cold water quench was approximately 0.8. For the less aggressive quenches the thermal gradients were expected to be smaller. The cooling curves recorded from the surface and centre locations (as shown in Figure 3) during the various quenching procedures are presented in Figure 11. These curves are representative of multiple repeated quenching experiments. Ulysse²⁷ has shown that surface finish can have a significant influence on cooling rate with an oxidised (akin to anodised) surface increasing the heat transfer coefficient by increased radiation through the vapour jacket, promoting unstable film boiling and then accelerating the transition from film boiling to nucleate boiling. To prevent this affecting the cooling curve data, the surface of the instrumented block was abraded with 600 grit SiC paper prior to every quench. The differences in the cooling curves due to the water temperature and quench media are apparent. Both PAG concentrations resulted in slower cooling than the cold water and water at 60°C. The boiling water quenched sample initially cooled very slowly with cooling accelerating as the vapour jacket breaks down at ~250°C. The figure also illustrates the difference in cooling rate for the two locations in the blocks. The surfaces cooled significantly quicker than the core for all samples except the boiling water quenched sample.

The influence of these varying cooling rates upon properties like yield strength and indentation hardness can be predicted using quench factor analysis. Evancho and Staley²⁸ described the time temperature property C-curve by an equation of the form:

$$C(T) = -k_1 k_2 \exp\left(\frac{k_3 k_4^2}{RT(k_4 - T)^2}\right) \exp\left(\frac{k_5}{RT}\right) \quad (4)$$

Where, $C(T)$ = critical time required to precipitate a constant amount of solute (s), k_1 = constant which equals the natural logarithm of the fraction untransformed during quenching, k_2 = constant related to the reciprocal of the number of precipitate nucleation sites (s), k_3 = constant related to the energy required to form a precipitate nucleus (J.mol⁻¹), k_4 = constant related to the solvus temperature of the second phase (K), k_5 = constant related to the activation energy for diffusion (J.mol⁻¹), R = Gas constant (J.mol⁻¹.K⁻¹) and T = Temperature (K). To predict the mechanical property (Hardness, Strength, etc.) the following equation was used:

$$\left(\frac{\sigma - \sigma_{\min}}{\sigma_{\max} - \sigma_{\min}}\right) = \exp(k_1 Q) \quad (5)$$

Where, Q = quench factor, σ_{\min} = minimum achievable property value, σ_{\max} = maximum achievable property value, σ = predicted property value. As $\sigma_{\min} \ll \sigma_{\max}$ in high strength alloys, Evancho and Staley let $\sigma_{\min} = 0$ to simplify the calculations. The quench factor can be determined from the following equation:

$$Q = \int_{t_0}^{t_f} \frac{dt}{C(T)} \quad (6)$$

Where t is time (s), t_0 = time at the start of the quench (s), t_f = quench finish time (s) and $C(T)$ is the critical time as a function of temperature; the loci of the critical times is the time temperature property (TTP) C-curve. Typically using a large number of specimens, cooling curves are recorded during the quench and the k_2 - k_5 parameters are iteratively changed to minimise the difference between the predicted and measured properties. The accuracy of this method was limited to the upper 10% of the strength of the alloy. A model to predict the properties down to levels lower than this was developed by Staley and Tiryakioglu²⁹. This model assumes that the material loses an incremental amount of ability to develop the property, $\Delta\sigma_j$, over each time interval, Δt_j such that:

$$\Delta\sigma_j = (\sigma_{j-1} - \sigma_{\min(T_j)}) \left[1 - \exp\left(-\frac{\Delta t_j}{C(T)}\right) \right] \quad (7)$$

Where, $\Sigma_{j-1} + \Delta\sigma_j = \sigma_j$

$\Delta\sigma_j$ = Incremental amount of strength loss, Δt_j = Time interval (s), $\sigma_{\min(T)}$ = minimum strength. $\sigma_{\min(T)}$ is a function of the equilibrium concentration at each temperature. For each subsequent incremental isothermal step, $\sigma_{j-1} = \sigma_{\min(T)}$ is a function of the amount transformed during the previous incremental isothermal step.

σ at the end of the quench can then be found by subtracting the sum of the $\Delta\sigma_j$'s from σ_{\max} :

$$\sigma = \sigma_{\max} - \sum_{j=1}^{j=n} \Delta\sigma_j \quad (8)$$

The time temperature indentation hardness curves for 7449 in an overaged condition (6 hours at 120°C and 10 hours at 160°C) were developed following the method of Staley and Tiryakioglu²⁹ and a Jominy end quench procedure detailed in Flynn and Robinson³⁰. The k_2 - k_5 and σ_{\max} and σ_{\min} constants for 7449 in this temper so determined are listed in Table 4.

Table 4. Constants for the TTP curve equation of the indentation hardness strength for a 7449T7x* forged block. (*6 hours at 120°C + 10 hours at 160°C)

| | k_2 (s) | k_3 (J.mol ⁻¹) | k_4 (K) | k_5 (J.mol ⁻¹) | σ_{\max} (HV20) | σ_{\min} (HV20) |
|---------------|------------------------|---------------------------------|--------------|---------------------------------|---------------------------|---------------------------|
| 7449 (T7x) | 2.01x10 ⁻¹¹ | 963 | 778 | 130066 | 192 | 42 |

These constants were used with Equation 4 to plot the iso-hardness curves present in Figure 11. What is confirmed from these data is that all the quenches except the boiling water are fast enough for this geometry to prevent significant loss of strength. This was confirmed by hardness measurements made at the centre of the d^0 strain free samples (as shown in Figure 4). The only sample significantly softer than the cold water quenched and overaged condition (185±5 HV20) was the boiling water quenched sample which had a hardness of 155±5 HV20.

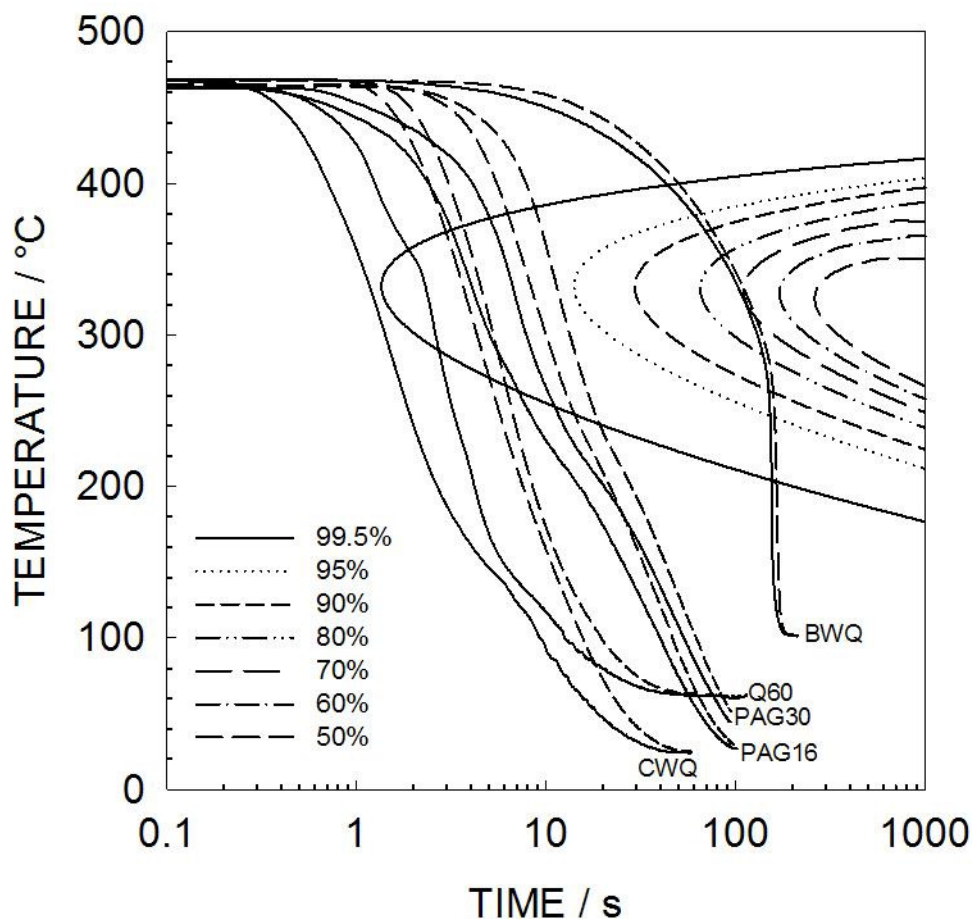


Figure 11. Cooling curves pairs for the surface and core of the blocks during quenching. The solid cooling curves correspond to the core, and the dashed the surface. Superimposed are time temperature transformation curves for the 7449 alloy. Each TTP curve represents an iso-hardness curve for the over aged condition that can produce the proportion of the hardness of a cold water quenched and aged sample as indicated in the legend.

Tensile properties

The different quenching procedures were expected to have a detrimental influence on the tensile properties relative to the cold water quenched sample. This is illustrated in Figure 12 where the 0.1% proof stress for each block is reported. The cold water, boiling water, water at 60°C and both PAG concentration samples were tested in both the naturally aged condition (which was the condition the neutron diffraction measurements were made in) and also additional samples were over aged to elucidate the influence of the slower quenching on the subsequent aging response.

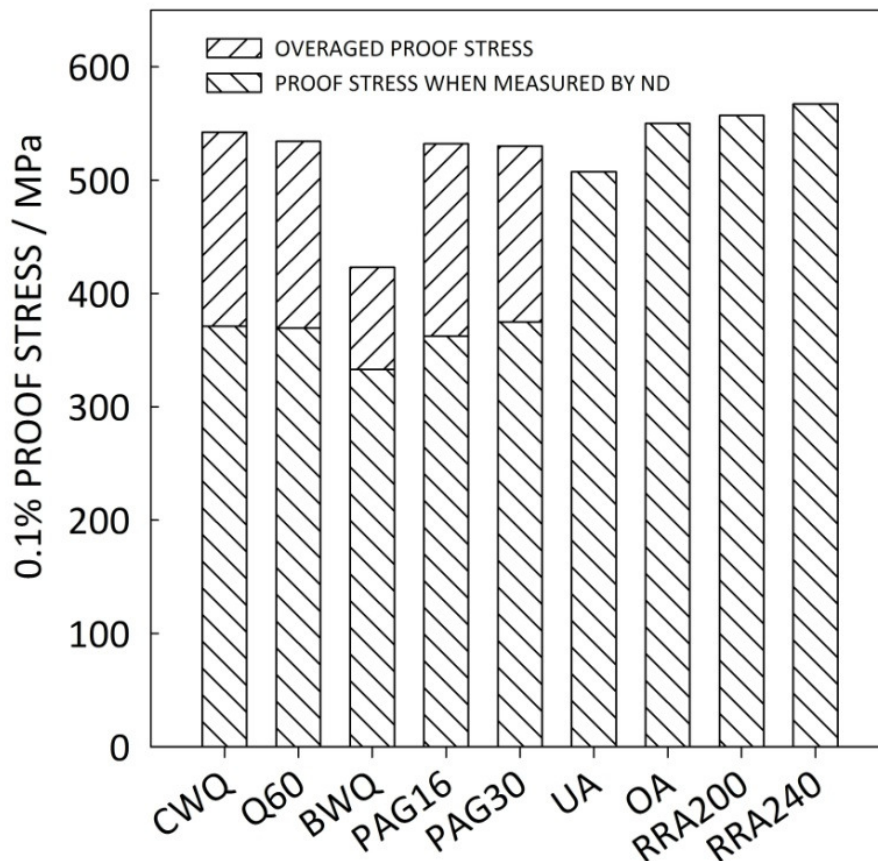


Figure 12. The 0.1% proof stresses ($R_{p0.1}$) of the blocks. The proof stresses of the CWQ, Q60, BWQ, PAG16 and PAG30 conditions were tested in the naturally aged and overaged condition. (See Table 2 for HT code). Uncertainties in the 0.1% proof stress were ± 10 MPa.

After 100 days of natural aging the 0.1% proof stresses were all quite similar except for the boiling water quenched condition which was significant softer. When subsequently overaged, the strengths increased. In Figure 12 the CWQ and OA conditions are in effect the same except the sample labelled CWQ had the benefit of 100 days natural aging prior to being artificially aged. This did not cause a significant difference in the proof stress.

Discussion

Influence of quenching on residual stresses

Characterisation of the residual stresses in the cold water quenched block X1A1 is consistent with the typically reported pattern of surface biaxial compression balanced by subsurface triaxial tension. The magnitude and distribution of these residual stresses were in good agreement with other investigations made by Robinson, Hossain et al.²⁶ on other neutron diffractometers using larger but similarly treated 7449 blocks. Steep residual stress gradients were present in the surfaces and complementary surface measurements using x-ray diffraction correlated well with the extrapolated neutron diffraction data. As expected, cold water quenching induced the largest magnitude residual stresses but also attained high tensile properties when overaged.

Quenching into warm water is a common industrial practice. The reason for this, as reported by Totten and Mackenzie³¹, is that when quenching at 55°C and below, local nucleate boiling areas can coexist on the surface with

film boiling in adjacent areas, giving local variations in hardness and issues with distortion, particularly in thin gauge products. It was found here that quenching into water at 60°C did result in a significant reduction in residual stress, although this data did not follow the same pattern as other blocks and the surface neutron diffraction measurements exhibited lower compressive stresses than expected. The surface x-ray measurement was more in line with the expected residual stress reduction and was consistent with the neutron diffraction measurement made at position A (32% reduction compared to cold water quenching). Quenching into water at 60°C did not adversely affect the hardness or tensile properties after aging when compared to the cold water quenched condition. This was primarily due to the low quench sensitivity of 7449. For the same reason the hardness and tensile properties of the PAG quenched samples were also good, as the cooling in these samples was similar to the material quenched at 60°C. Here the additional benefit of PAG quenching can be clearly seen in that there was a larger reduction in residual stress for both PAG concentrations. Adding PAG to water increases the viscosity of the quenchant (into a treacle like consistency at about 40%), but PAG actually modifies cooling during quenching by reducing the duration of the vapour jacket stage (film boiling) by immediately coating the workpiece in a film of concentrated PAG, thus allowing heat transfer through the layer by conduction, and permitting wetting and subsequent nucleate boiling to occur at the exterior surface of this layer. A recent description of the technology of PAG quenching is provided by Croucher³². There was a small but detectable reduction in the cooling rate when the concentration of PAG was increased from 16% to 30%. The neutron diffraction residual stress characterisation was sensitive enough to be able to detect the consequences of this with PAG 16% resulting in a 45% reduction, and PAG 30% a 56 % reduction in residual stress at position A relative to CWQ. Boiling water quenching was very effective in eliminating residual stress almost completely for this geometry. However the penalty of the boiling water quench was a 22% reduction in the over aged 0.2% proof stress and a 14% reduction in the indentation hardness compared to the CWQ+OA condition. Nevertheless, boiling water quenching is a common commercial process for certain aluminium alloys and used where residual stresses cannot be tolerated.

Heat transfer during quenching

The influence of the different quenching regimes investigated here can be better displayed by determining the time transient heat transfer coefficient. Figure 13 illustrates how the heat transfer coefficient of the Al-Cu-Mg alloy 2014A varies with excess temperature (temperature above that of the quenchant) when quenched from 500°C into cold, boiling, and water at 60°C, and the two concentrations of PAG. This data was generated using a 160 mm diameter, 21 mm thick solid disc. A thermocouple was inserted into a blind hole in the centre of the disc face. The hole had been drilled to within 0.5 mm of the surface of the opposite side of the disc. The edge of the disc was insulated using a stainless steel band. Heat was therefore considered to be lost in only one direction, normal to the circular surfaces of the disc. The direction of heat flow was assumed to be from the centre of the disc to these surfaces. Time temperature histories during quenching were used as a boundary condition in a one-dimensional finite element model. The model was constructed using the software INTEMP created by Trujillo³³, and this numerically solved the inverse heat conduction problem to give the unknown heat fluxes and heat transfer coefficients using the procedure described by Busby and Trujillo³⁴. The finite element model had 21 nodes from the centre to the surface of the disc. Values for the specific heat capacity, thermal conductivity and density of 2014A (which differ little to 7449), as a function of temperature, were extracted from the literature of Touloukian, Powell et al.³⁵. Changes in the slope in these curves are mainly due to the vigorous agitation. This can also account for the heat transfer coefficients being larger than other investigations, an example of which are the experiments of Ulysse and Schultz³⁶.

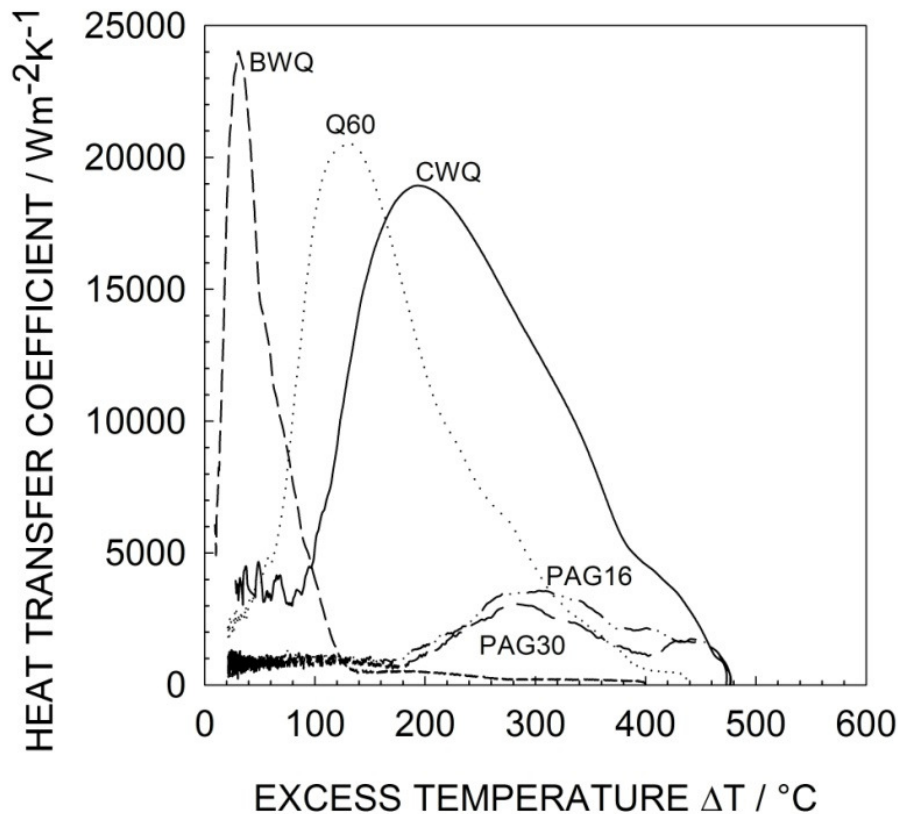


Figure 13. Heat transfer coefficient for the alloy 2014 quenched into cold (CWQ), boiling (BWQ), and water at 60°C (Q60), a 16% PAG solution (PAG16) and a 30% PAG solution (PAG30).

Cold water quenching and quenching at 60°C both result in large heat transfer coefficients over the complete quenching range until the temperature falls below 100°C when convection takes over. Boiling water quenching is dominated by the formation of a stable and persistent vapour jacket. This film boiling results in very limited heat transfer until the temperature falls below the point referred to as the Leidenfrost temperature. At this point the vapour jacket collapses and very vigorous nucleate boiling commences. This is reflected in the large but short lived heat transfer coefficient at around 250°C. What is clearly demonstrated by Figure 13 is the quite different way that heat is transferred by the PAG solutions. The heat transfer coefficient arising from the PAG quenches results in heat being extracted much more slowly in the initial stages of quenching. This is the regime of cooling where it has been reported by Nicol, Seaton et al.³⁷ that residual stress formation due to surface plastic deformation occurs.

Influence of aging on residual stress

Artificial aging of 7449 results in precipitation of GP zones and the transition precipitate η' and eventually the equilibrium precipitate η (MgZn_2). The increases in hardness and electrical conductivity (measured in % IACS (International Annealed Copper Standard), where 100% IACS = 58 MS m^{-1}) during aging at 120 and then 160°C are shown in Figure 14. Both the underaged condition and overaged conditions investigated here did result in a residual stress reduction but it was small and in practical terms, of little consequence. The same was true of both retrogression and reaging treatments investigated. The short duration excursion to elevated temperatures during the retrogression treatment does appear to produce a very small additional stress relief compared to the UA and OA conditions, but again is little benefit when compared to the stress relief obtainable by modifying the quench regime or indeed subsequent mechanical stress relief.

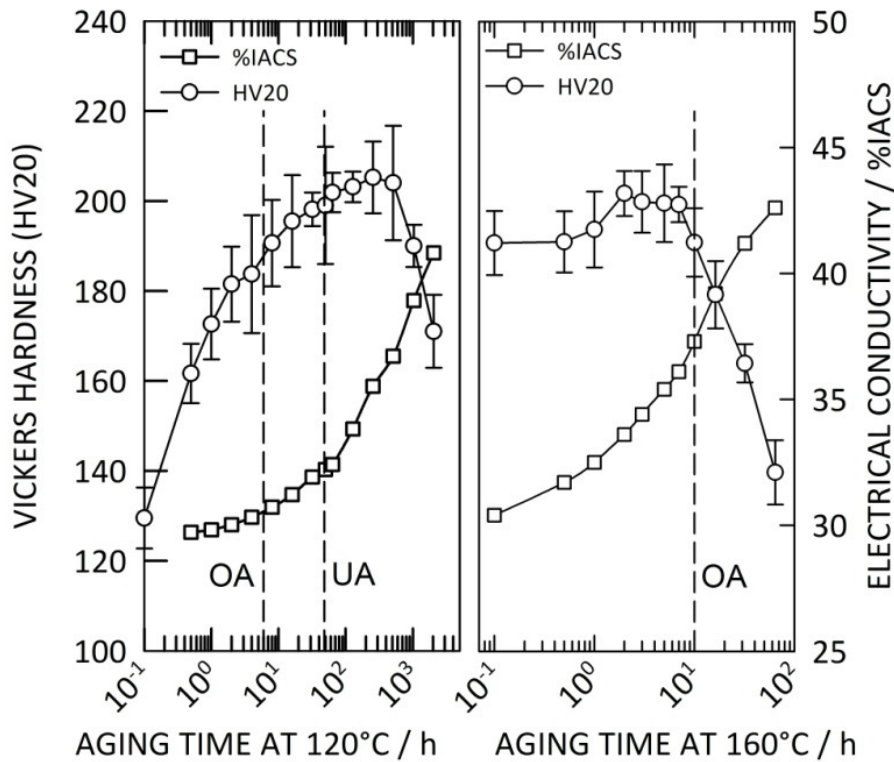


Figure 14. Aging behaviour of 7449 at 120°C and 7449 after receiving 6 h at 120°C and then subsequently aged at 160°C.

Quench factor analysis

Microstructural variation arising from precipitation reactions causes the large changes in the strain free lattice parameter as illustrated in Figure 8. When characterising the residual stresses present in thick aluminium alloy components one must be cognisant of the consequences of this, especially if the strain free reference does not reflect the extremes of the range of cooling paths the material is exposed to during quenching. If the strain free reference is sectioned from a location that is cooled rapidly, for example close to a surface, corner or edge, then its lattice parameter could be quite different from a strain free reference taken from a more slowly cooled region due to precipitation occurring. Being able to estimate this variation is desirable, as the residual stress investigator is at least, better informed about the suitability of the strain free reference to reflect the microstructural condition of the whole component. The change in lattice parameter arising from microstructural change can be estimated using quench factor analysis (QFA). In this investigation the only quench path that would have been expected to give rise to a large change in the lattice parameter was boiling water. (The quench factors, Q in equation 6, of the centre locations of the CWQ, Q60, PAG16, PAG30 and BWQ samples were 2.2, 3.1, 5.6, 6.7 and 51.0 respectively.)

Quench factor analysis of the BWQ sample indicated that the indentation hardness when overaged should be 80% of the hardness of the cold water quenched and overaged sample. (Measurement confirmed the actual hardness to be 84% of the CWQ+OA hardness). If it is assumed that the potential to develop hardness is related to the amount of solute retained in solid solution which in turn influences the lattice parameter, then the predicted lattice parameter is within the equivalent of 100 $\mu\epsilon$ of the actual measured lattice parameter. In practical terms this means that for this investigation it was actually unnecessary to manufacture stress free samples from the Q60, PAG16 and PAG30 samples as the CWQ lattice parameter would have sufficed for these, and for the BWQ sample the QFA prediction was acceptably close to the actual value.

Conclusions

Cold water immersion quenching rectilinear blocks of the aluminium alloy 7449 induced tensile triaxial residual stresses in the central regions of the sample balanced by surface biaxial compressive residual stresses. The stress magnitudes varied significantly with the orthogonal measurement directions.

Steep residual stress gradients were identified in the surfaces of the cold water quenched sample and extrapolated neutron diffraction residual stresses correlated well with complementary x-ray diffraction observations.

Modification of the cooling rate during quenching was found to have a significant influence on the residual stresses. Quenching into water at 60°C, PAG at concentrations of 16% and 30%, and boiling water all resulted in slower cooling and consequently lower residual stress.

Artificial aging to achieve under and over aged conditions following cold water quenching resulted in small but detectable reductions in residual stress (<30%). Similar reductions were observed when samples were retrogressed and reaged, again following cold water quenching.

The impact of the different quenching regimes on the strength of the alloy was quantified and found to be only significant for the sample quenched into boiling water (slowest cooling). That quenching into warm water and PAG had such a minor effect on strength is a reflection on the relatively small sample size investigated and the fact that 7449 is not a very quench sensitive alloy.

Of the alternative quench regimes investigated, quenching into a 30% PAG solution gave the best compromise between achieving high tensile properties and minimising the residual stress.

If time temperature property data (C curve) is available for a precipitation hardened aluminium alloy in conjunction with cooling curve data for the locations of interest, an established modified quench factor analysis can be used to predict the lattice parameters arising from different quench paths. This has been demonstrated to accurately predict the lattice parameter of boiling water quenched and overaged samples of the forged aluminium alloy 7449.

Acknowledgements

This investigation has been supported by the European Commission under the 6th Framework Programme project known as COMPACT (AST4-CT-2005-516078), which contributes to the thematic priority "Strengthening Competitiveness" of the European aircraft industry. This work is based on experiments performed on the POLDI instrument at the Swiss spallation neutron source SINQ, Paul Scherrer Institute, Villigen, Switzerland. The neutron diffraction measurements were also supported by the European Commission under the 7th Framework Programme through the 'Research Infrastructures' action of the 'Capacities' Programme, Contract No: CP-CSA_INFRA-2008-1.1.1 Number 226507-NMI3'. The authors are also grateful for the contribution of Mettis Aerospace Ltd., UK.

References

1. R. E. Kleint and F. G. Janney: 'Stress Relief in Aluminum Forgings', *Light Metal Age*, 1958, **2**, 14-21.
2. R. Becker, M. E. Karabin, J. C. Liu, and R. E. Smelser: 'Distortion and residual stress in quenched aluminum bars', *Journal of Applied Mechanics-Transactions of the Asme*, 1996, **63**(3), 699-705.
3. P. Jeanmart and J. Bouvaist: 'Finite element calculation and measurement of thermal stresses in quenched plates of high-strength 7075 aluminium alloy', *Mater. Sci. Technol.*, 1985, **1**, 765-769.
4. S. R. Yazdi, D. Retraint, and J. Lu: 'Study of through-thickness residual stress by numerical and experimental techniques', *J. Strain Anal. Eng. Des.*, 1998, **33**(6), 449-458.
5. D. M. Walker and R. Y. Hom: 'Residual stress analysis of aircraft aluminum forgings', *Adv. Mater. Process.*, 2002, **160**(6), 57-60.
6. G. M. Orner and S. A. Kulin: 'Development of stress relief treatments for high strength aluminum alloys', Manlabs Inc. , Massachusetts, 1965.
7. Y. Altschuler, T. Kaatz, and B. Cina: 'Mechanical Relaxation of Residual Stresses', in 'ASTM STP 993', 19-29; 1988.
8. W. E. Nickola: 'Residual Stress Alterations via Cold Rolling and Stretching of an Aluminum Alloy', in 'ASTM STP 993', 7-18; 1988.
9. M. Koc, J. Culp, and T. Altan: 'Prediction of residual stresses in quenched aluminum blocks and their reduction through cold working processes', *Journal of Materials Processing Technology*, 2006, **174**(1-3), 342-354.

10. D. A. Tanner, J. S. Robinson, and R. L. Cudd: 'Relief of residual stresses in aluminium alloy 7010', in 'Proceedings of the The Sixth International Conference on Residual Stresses ICRS-6, 10-12 July 2000', 1299-1306; 2000, Oxford, UK, Institute of Materials.
11. J. R. Davis, G. M. Davidson, and S. R. Lampman: 'Heat treating of aluminum', 841-879; 1995, ASM International.
12. B. Cina, I. Kaatz, and I. Elror: 'The effect of heating shot peened sheets and thin plates of aluminium alloys.', *J. Mater. Sci.*, 1990, **25**, 4101-4105.
13. J. T. Staley: 'Quench factor analysis of aluminium alloys', *Mater. Sci. Technol.*, 1987, **3**, 923-935.
14. M. E. Fitzpatrick, A. T. Fry, P. Holdway, F. A. Kandil, J. Shackleton, and L. Suominen: 'Determination of residual stresses by X-ray diffraction', 52, NPL, 2002.
15. I. C. Noyan and J. B. Cohen: 'Residual Stress [Measurement by Diffraction and Interpretation]', in 'Residual Stress [Measurement by Diffraction and Interpretation]', 1987, New York, Springer-Verlag.
16. V. M. Hauk and E. Macherauch: 'A useful guide for X-ray stress evaluation (XSE)', *Advances in X-ray Analysis*, 1983, **27**, 81-89.
17. B. D. Cullity and S. R. Stock: 'Elements of x-ray diffraction'; 2001, Upper Saddle River, New Jersey, USA, Prentice Hall.
18. U. Stuhr, M. Grosse, and W. Wagner: 'The TOF-strain scanner POLDI with multiple frame overlap-concept and performance', *Mater. Sci. Eng. A-Struct. Mater. Prop. Microstruct. Process.*, 2006, **437**(1), 134-138.
19. J. M. Drezet and A. B. Phillion: 'As-Cast Residual Stresses in an Aluminum Alloy AA6063 Billet: Neutron Diffraction Measurements and Finite Element Modeling', *Metall. Mater. Trans. A-Phys. Metall. Mater. Sci.*, 2010, **41A**(13), 3396-3404.
20. ISO/TTA3: 'Polycrystalline materials – Determination of residual stresses by neutron diffraction', ISO/TTA3, International standardisation organisation, 2001.
21. D. C. I. T. 21432: 'Non-destructive testing. Standard test method for determining of residual stresses by neutron diffraction', DD CEN ISO/TS 21432, British Standards Institute, 2005.
22. G. A. Webster and R. C. Wimpory: 'Non-destructive measurement of residual stress by neutron diffraction', *Journal of Materials Processing Technology*, 2001, **117**(3), 395-399.
23. G. S. Pawley: 'Unit-cell refinement from powder diffraction scans', *J. Appl. Crystallogr.*, 1981, **14**(DEC), 357-361.
24. M. T. Hutchings, P. J. Withers, T. M. Holden, and T. Lorentzen: 'Introduction to the characterisation of residual stress by neutron diffraction', 424; 2005, Boca Raton, FL, USA, CRC Press.
25. A. Steuwer, M. Dumont, M. Peel, M. Preuss, and P. J. Withers: 'The variation of the unstrained lattice parameter in an AA7010 friction stir weld', *Acta Mater.*, 2007, **55**(12), 4111-4120.
26. J. S. Robinson, S. Hossain, C. E. Truman, E. C. Oliver, D. J. Hughes, and M. E. Fox: 'Influence of cold compression on the residual stresses in 7449 forgings', *Advances in X-ray Analysis*, 2009, **52**, 667-674.
27. P. Ulysse: 'Thermo-mechanical characterization of forged coated products during water quench', *Journal of Materials Processing Technology*, 2009, **209**(15-16), 5584-5592.
28. J. W. Evancho and J. T. Staley: 'Kinetics of Precipitation in Aluminium Alloys During Continuous Cooling', *Metallurgical Transactions*, 1974, **5**(Jan), 43-47.
29. J. T. Staley and M. Tiryakioglu: 'The use of TTP curves and quench factor analysis for property prediction in aluminum alloys', Proceedings from Materials Solutions Conference 2001, Nov 5-8 2001, Indianapolis, IN, United States, 2001, ASM International, 6-15.

30. R. J. Flynn and J. S. Robinson: 'The application of advances in quench factor analysis property prediction to the heat treatment of 7010 aluminium alloy', Proceedings of the International Conference on Advances in Materials and Processing Technologies, AMPT2003, Dublin City University, Dublin, Ireland, 8-11 July 2003, 2003, 123-126.
31. G. E. Totten and D. S. Mackenzie, eds. *Handbook of Aluminum: Volume 1. Physical Metallurgy and Processes*, Vol. 1, 2003, New York, Basel, Marcel Dekker Inc.
32. T. Croucher. 'Effectively quenching thick sections of high strength aluminum alloys using polyalkylene glycol quenchants', 2009 [viewed; Available from: <http://www.croucher.us/articles/thick-sections>].
33. D. M. Trujillo, *INTEMP*. 2003, TRUCOMP: FOUNTAIN VALLEY, CA., 92708, USA. p. Inverse Heat Transfer Analysis.
34. H. R. Busby and D. M. Trujillo: 'NUMERICAL-SOLUTION TO A 2-DIMENSIONAL INVERSE HEAT-CONDUCTION PROBLEM', *International Journal for Numerical Methods in Engineering*, 1985, **21**(2), 349-359.
35. Y. S. Touloukian, R. W. Powell, C. Y. Ho, and P. G. Klemens: 'Thermal Conductivity: Metallic elements and alloys', in 'Thermophysical properties of matter', 1970, New York, IFI/Plenum Press.
36. P. Ulysse and R. W. Schultz: 'The effect of coatings on the thermo-mechanical response of cylindrical specimens during quenching', *Journal of Materials Processing Technology*, 2008, **204**(1-3), 39-47.
37. J. A. Nicol, E. D. Seaton, G. W. Kuhlman, H. Yu, and R. Pishko: 'New quenchant for aluminum', *Adv. Mater. Process.*, 1996, **149**(4), S40.